NANO LETTERS

pubs.acs.org/NanoLett Letter

Electrothermoplasmonic Trapping and Dynamic Manipulation of Single Colloidal Nanodiamond

Chuchuan Hong, Sen Yang, Ivan I. Kravchenko, and Justus C. Ndukaife*

Cite This: https://doi.org/10.1021/acs.nanolett.1c00357 Read Online

ACCESS | Metrics & More | Article Recommendations | Supporting Information

ABSTRACT: Low-power trapping of nanoscale objects can be achieved by using the enhanced fields near plasmonic nanoantennas. Unfortunately, in this approach the trap site is limited to the position of the plasmonic hotspots and continuous dynamic manipulation is not feasible. Here, we report a low-frequency electrothermoplasmonic tweezer (LFET) that provides low-power, high-stability and continuous dynamic manipulation of a single nanodiamond. LFET harnesses the combined action of the laser illumination of a plasmonic nanopillar antenna array and low-frequency alternating current (ac) electric field to establish an electrohydrodynamic potential capable of the stable trapping and dynamic manipulation of single nanodiamonds. We experimentally demonstrate the fast transport, trapping, and dynamic manipulation of a single nanodiamond using a low-frequency ac field below 5 kHz and low-laser power of 1 mW. This nanotweezer platform for nanodiamond manipulation holds promise for the scalable assembly of single photon sources for quantum information processing and low noise quantum sensors.

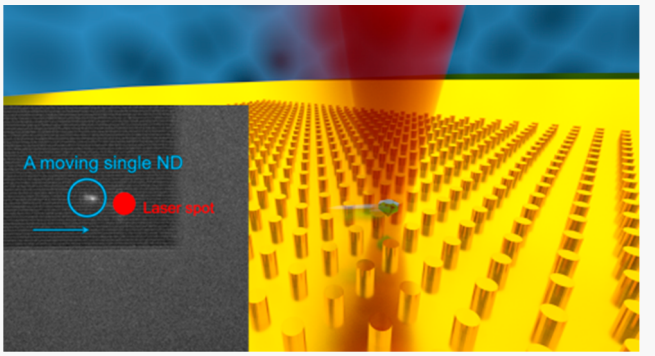

KEYWORDS: *nanotweezers, photothermal effect, electrohydrodynamics, nanodiamond*

Plasmonic nanoantennas, which can confine and enhance local electromagnetic fields, are a powerful platform for the development of optical nanotweezers.[1−5] Upon resonant illumination, plasmonic nanoantennas create highly localized and enhanced electromagnetic fields within volumes well-beyond the diffraction-limit[6,7] and thus produce narrower and deeper trapping potential wells than the conventional optical tweezers. This capability facilitates trapping nanoscale particles using relatively low laser power with high stability.[8−10] The use of optical forces from plasmonic nanoantennas is particularly suited for the trapping and positioning of colloidal nanodiamonds (NDs) near plasmonic cavities to enhance the light−matter interaction. In particular, for quantum photonics applications NDs have been identified as stable quantum emitters[11−13] capable of providing single photon emission under room-temperature conditions.[14] To enhance their emission properties, it is crucial to develop methods that can rapidly trap and couple them to respective nanophotonic cavities. Because of their small sizes, NDs are more accessible for trapping using plasmonic nanotweezers in comparison to the conventional optical tweezers. However, on-chip plasmonic nanotweezers are only able to trap the nanoscale objects at the specific position of the hotspot defined by the plasmonic nanoantenna and do not possess dynamic manipulation capability along the plasmonic substrate. Prior work by Lin et al.[15] reported the continuous dynamic manipulation of single nanoscale charged gold nanoparticles using a thermoelectric field induced by the photothermal heating of a porous gold plasmonic substrate submerged in an ionic surfactant. In this approach, ionic surfactants (cetyltrimethylammonium chloride) are introduced in the colloidal solution, which in the presence of a thermal gradient establishes the attractive thermophoretic force to enable the trapping of the gold colloids with single particle resolution. This approach has yet to be translated to the continuous dynamic manipulation of single nanoscale dielectric objects.[15−18] Another recently reported technique by Gosh et al. employs dielectric microrods that are coated with plasmonic nanodisks.[19] The dielectric microrods are large enough to be optically trapped with conventional optical traps, while the light coupled to the plasmonic nanodisks serves as plasmonic tweezers that can trap the nanoscale objects in solution. Dynamic manipulation of the trapped nanoscale objects is achieved in an indirect fashion by manipulating the optically trapped dielectric microrods.

Here, we capitalize on the latest advances in electrothermoplasmonic tweezers[20−22] and present a method termed

Received: January 26, 2021
Revised: May 29, 2021

https://doi.org/10.1021/acs.nanolett.1c00357
Nano Lett. XXXX, XXX, XXX−XXX

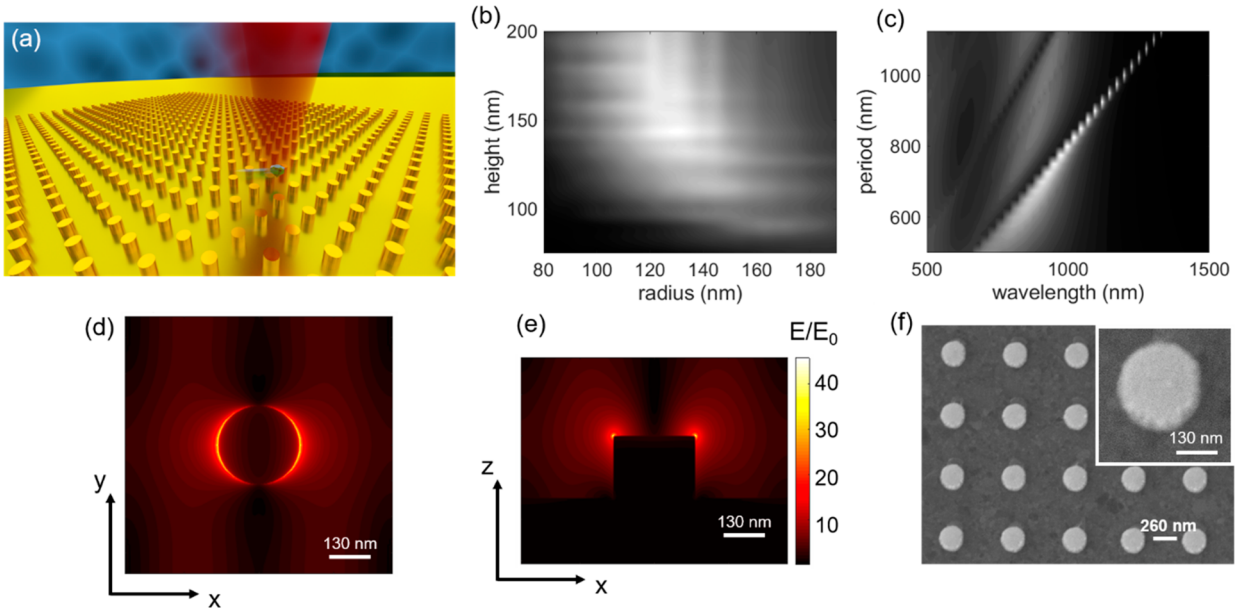

Figure 1. (a) Three-dimensional illustration of the ac-assisted nanotweezer enabled by an array of plasmonic nanoantenna capable of dynamic manipulation of single nanodiamonds. A single nanodiamond is trapped and repositioned by the laser motion relative the nanoantenna array. (b) The absorption cross section efficiency map obtained from sweeping the radius and height of the gold nanopillars in an array. (c) The absorption cross section efficiency spectra when we parametrically sweep the lattice constant of an infinite array. The resonance wavelength is tuned to 973 nm. (d) The simulated electric field distribution in one unit-cell on the top of the nanopillar. (e) The simulated vertical electric field distribution in one unit-cell across the center of the nanopillar. In (d,e), the plane-wave excitation is along the *z*-direction with a 973 nm wavelength. The color bar is normalized by the incident light electric field amplitude. (f) The SEM image of the fabricated gold-nanopillar array.

low frequency electrothermoplasmonic tweezer (LFET) that uses low-frequency alternating current (ac) electric field combined with a laser illumination for the trapping and continuous dynamic manipulation of a single ND (70−100 nm in diameter) suspended in deionized water environment. Using LFET, we can trap a single ND on the top of an array of a plasmonic nanoantenna and dynamically manipulate the single ND by simply moving the laser spot or microscope stage, as shown in Figure 1a. Our nanotweezers platform is composed of an array of gold nanopillars illuminated with a near-IR laser (973 nm wavelength) and perpendicularly applied low-frequency ac electric field to optically induce thermal gradients and distort the ac electric field, respectively. To obtain a maximized photothermal conversion efficiency, while keeping the laser power low, we parametrically optimize the absorption cross section of one unit-cell by sweeping the radius, height, and lattice constant of the gold nanopillar array, as shown in Figure 1b,c. The coupling of the gold nanopillar array and the induced localized plasmon resonance of the single antennas results in an enhanced and spatially confined electric field distribution, as shown in Figure 1d,e, so that the photothermal conversion efficiency is enhanced. The optimized gold nanopillars are of 130 nm in radius and 150 nm in height and are placed on a 50 nm thick gold film on a glass substrate. The lattice constant of the array is 720 nm, which ensures that the highest absorption cross section is centered around 973 nm wavelength. We also notice that tuning the size and period of the gold nanopillar does not have a significant effect on the distribution of the applied ac electric field as shown in Figures S1 and S2. We attribute this to the fact that the wavelength of the ac field is much larger than the tuning range of the size and period of the gold nanopillar. As a result, the optically optimized design with a radius of 130 nm and period of 720 nm was chosen for this work. The scanning electron microscopy (SEM) image of the fabricated sample is depicted in Figure 1f. The fabrication was performed using the standard nanofabrication approach composed of electron-beam lithography and lift-off (see Methods).

Using the optimized design, the absorption, reflection, and transmission spectra are numerically calculated and plotted in Figure 2a. The absorption cross-section is obtained by solving the Maxwell's equation using a finite-different-time-domain commercial solver, Lumerical FDTD. The enhanced light absorption leads to temperature rise and thermal gradient in the fluid. The simulated temperature that rises for a 1 mW laser illumination and focused to a spot size of 1 μm radius is depicted in Figure 2b. An ac electric field is applied across the microfluidic channel to establish the electrothermoplasmonic (ETP) flow because of the action of the laser-induced thermal gradient and applied ac field, which enables fast transport and the in-plane manipulation of trapped NDs. The gold nanopillar array distorts the local ac electric field to create both normal and tangential ac electric-field components. These tangential components exert lateral Coulombic force on the diffuse charges in the electrical double layer (EDL), which produces local ac electro-osmotic (ACEO) motion of the fluid. The total flow fields at a position of 50 nm above the array when the laser is focused at the center and off the center of the array are depicted in Figure 2c,d, respectively. They show the ability of our nanotweezers to reposition the trapping location site by relocating the laser spot on the gold nanopillar array. Additionally, the primary force responsible for the localization of the trapped nanodiamonds along the out-of-plane direction is due to the particle−surface interaction force, which results from the interaction between the surface charges of the particle and their image charges in the conducting plane.[23] This particle surface interaction force increases at lower ac frequencies below the charge relaxation frequency of the

https://doi.org/10.1021/acs.nanolett.1c00357
Nano Lett. XXXX, XXX, XXX−XXX

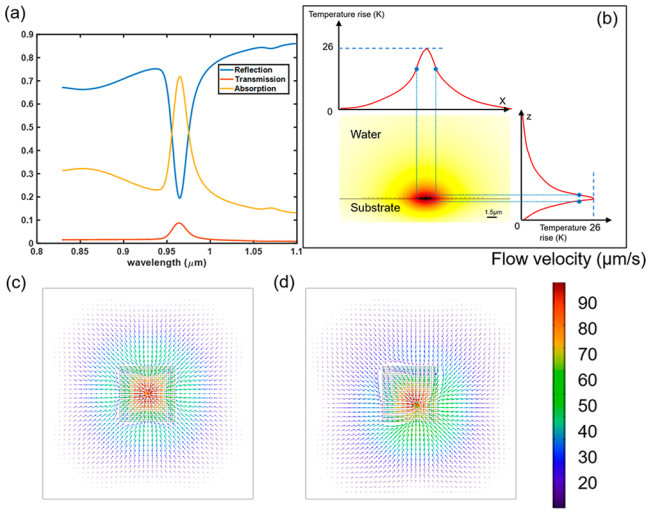

Figure 2. (a) The simulated absorption, reflection, and transmission spectra of an infinite array of gold nanopillar array. The absorption spectrum is centered at a peak wavelength of 973 nm to maximize the photothermal conversion efficiency at this wavelength. (b) The simulated temperature rise in the vicinity of the nanopillar array using 1 mW laser of 973 nm and 1 μm laser spot radius. Line plots indicate the thermal confinement is better along the vertical direction than along the horizontal direction because of thermal spreading into the high thermal conductivity gold film. The total flows including ACEO and ETP flows simulated using the same laser settings as (b) with the laser spot at (c) the center of the array and (d) off from the center of the array. The induced temperature field from (b) in conjunction with an applied ac electric field generates a strong ETP flow centered around the laser spot position. By moving the laser position, the flow fields are spatially translated along the plasmonic substrate.

fluid. The interplay between the microfluidic flows, optical gradient force, and particle−surface interaction force enhanced at low ac electric-field frequencies enables the rapid particle loading process, localization of a single ND near the gold nanopillar array, and dynamic manipulation of a single ND. A detailed explanation of the respective contributions of the forces acting on a single nanodiamond in the system is presented in the Supporting Information along with the numerical analysis of the particle−surface interaction force, repulsive thermophoretic force, and optical gradient force. Furthermore, an illustration of the direction of the forces is depicted in Figure S3. The electrohydrodynamic physics to model the flows is simulated using the finite-element-solver in COMSOL Multiphysics software.

Experimental demonstration was performed using diluted solution of NDs (Sigma-Aldrich fluorescent nanodiamond) with an average particle size of 70−100 nm in deionized water. The NDs are diluted to a concentration of 5.65×10^5 particle/mL. A linearly polarized laser beam with 973 nm wavelength was focused to a spot size of 1 μm radius on the gold nanopillar array using a water immersion objective lens with a numerical aperture of 1.2. Figure 3a shows the process of fast transport, trapping, and releasing of a single ND particle under different ac frequencies, as shown in SI Video 1. The laser power was set to 1 mW and the ac frequency was initially set to a low frequency of 2 kHz to guarantee the trapping. First, we illuminated the nanopillar region with the laser but without the ac field applied and no trapping phenomenon was observed. Then an ac electric field at a frequency of 2 kHz was applied perpendicular to the gold film. The applied peak-to-peak voltage was 10 V and the microfluidic chamber height is 120 μm, corresponding to an ac electric field amplitude of 83 333

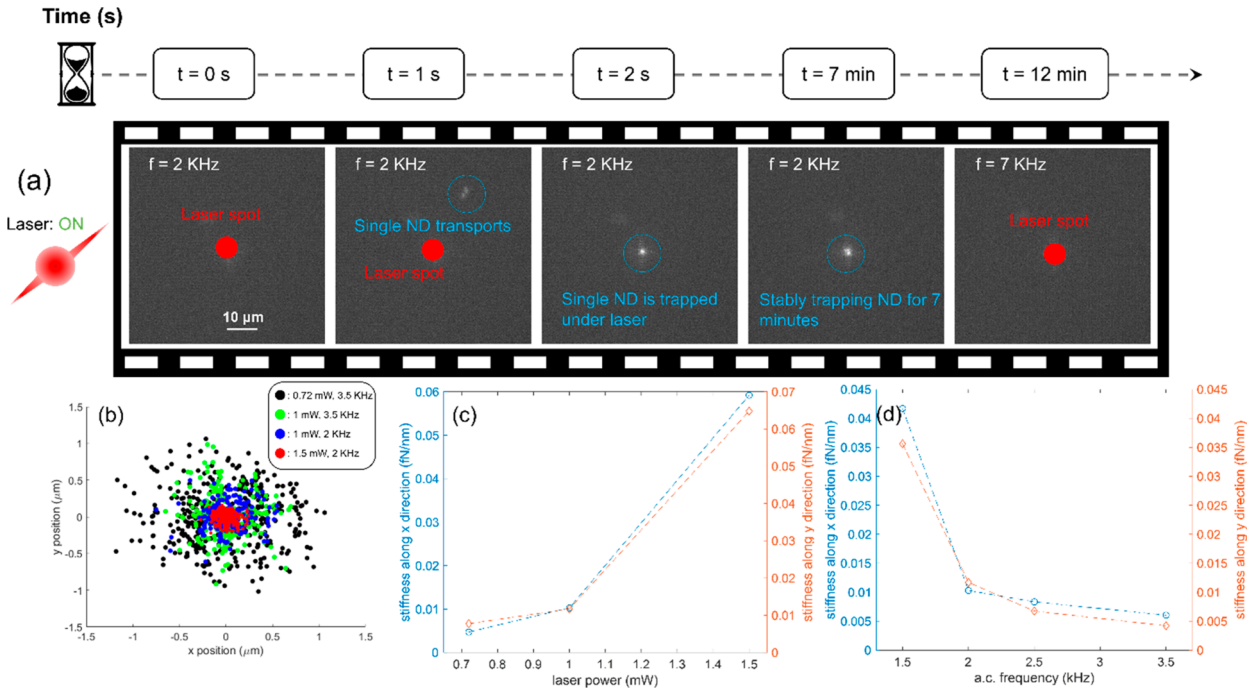

Figure 3. (a) The sequence of frames shows the fast process of a single ND transported into the hotspot and stably trapped on the gold nanopillar pattern for 7 min at 2 kHz. By tuning up the ac frequency to 7 kHz, the single ND is released rapidly. (b) The scattering plot of the trapped single ND under various ac field and laser power conditions. (c) The stiffness calculated at 2 kHz ac frequency with varying laser power applied. Higher laser power enables higher trapping stiffness. Blue circles represent the stiffness along the *x*-direction, and orange diamonds represent the stiffness along *y*-direction.

https://doi.org/10.1021/acs.nanolett.1c00357
Nano Lett. XXXX, XXX, XXX−XXX

V/m. Immediately, an ETP flow was generated inside the microchannel resulting in the rapid transport of a single ND to the illuminated gold nanopillar array region. These results contrast with our previous findings describing opto-thermo-electrohydrodynamic tweezers (OTET)[20] using a finite array of gold nanoholes. The difference in the particle trapping behavior for the nanopillar array versus the nanohole array arises because the distribution of the induced ac electro-osmotic flow field vectors act in a manner to induce a strong centripetal drag force (i.e., radially inward) on the nanoscale objects toward the nanopillar array. Furthermore, the nano-pillar array possesses a stronger radially inward ETP flow that acts to transport target objects toward the illuminated laser spot. Thus, unlike in OTET[20] the nanoscale objects are not repelled from the nanopillar array to establish a stagnation zone as depicted in Figure S5 (see Supporting Information). Upon arrival of the ND to the laser spot, it is stably trapped at the position of the laser illumination as long as the laser illumination and the low-frequency ac field are simultaneously present. After 7 min, the ac electric field frequency was increased from 2 to 7 kHz and the ND was rapidly released from the trap by the axial component of the ETP flow as depicted in Figure 3a. This is because the particle−surface interaction force reduces as the ac frequency is increased. Thus, the drag force from the axial ETP flow and the repulsive thermophoretic force overcomes the particle−surface inter-action force to convect the particle away from the surface of the nanopillar array.

The trapping stability under various laser power and ac frequency conditions are described in the scatter plots in Figure 3b. The trapping stability for the data presented in Figure 3a is depicted in blue. The trap stiffness was determined by using the equipartition theorem approach[24] as described in Section 4 of Supporting Information. Figure 3c depicts the trapping stiffness along the x- and y-direction under varying laser power conditions for a constant ac field frequency of 2 kHz. The results show that the trapping stiffness is increasing with increasing laser power. We attribute this enhancement in the in-plane trapping stiffness to the fact that the in-plane optical gradient force and the radial ETP flow drag force increases with higher laser power. The variation of the trapping stiffness with the applied ac frequency under a fixed laser power of 1 mW is depicted in Figure 3d The result shows an inverse relation whereby the trapping stiffness is increasing with decreasing ac field frequency. This is because for lower ac frequency, the particle−surface interaction force along the vertical direction and local ACEO flow are both strength-ened.[25,26] In general, as depicted in Figure 3b, the trapping stability increases with increasing laser power and decreasing ac field frequency. The laser power still needs to be kept within the limits that prevents excessive temperature rise to prevent laser-induced bubble formation. Thus, LFET provides the means to harness the synergistic interaction of optical gradient force and electrostatic particle−surface interaction force to achieve the stable trapping and dynamic manipulation of a single nanodiamond. It should be noted here that the gold nanopillar array provides strong electric field enhancement, which can enhance the optical gradient force and the photothermal heating of the gold nanopillar array. The photothermal heating of the gold nanopillar array gives rise to a positive (i.e., repulsive) thermophoretic force. This thermophoretic force is repulsive in the absence of ionic surfactants in the fluid medium and thus repels the suspended nanodiamond from the nanoantenna.[17,27] A quantitative analysis is presented in Section 7 of Supporting Information to show the contribution from the thermophoretic force that repels the nanodiamond from the surface of the gold nanopillars. We also performed experiments whereby the nanodiamond was initially trapped using the ac field and laser illumination. Subsequently, the ac field was turned off with the laser still on and the nanodiamond was observed to escape from the trap as shown in SI Video 3. This result suggests that the optical gradient force alone was not sufficient to stably trap the nanodiamond in the presence of the repulsive thermopho-retic force.

To investigate this further, we have calculated the repulsive thermophoretic force and optical gradient force along the z-direction (axial) as depicted in Figure S8. The result shows a peak thermophoretic force with a maximum of about 0.33 pN at the illumination power of 1 mW. We have compared the optical gradient force and repulsive thermophoretic force in the axial direction under varying laser powers ranging from 0.5 to 1.5 mW. The result presented in Figure S8b shows that the axial repulsive thermophoretic force is larger than the optical gradient force for all the laser powers considered. Thus, in the presence of laser illumination of the nanopillar array alone, the repulsive thermophoretic force would prevent the trapping of the nanodiamond with optical force alone. This repulsive thermophoretic force has been reported to prevent stable plasmonic optical trapping using plasmonic nanoantenna in earlier works unless the temperature rise is minimized such as by using very low optical illumination intensity,[28] off-resonant excitation,[29] or integrating a heat sink.[5] In LFET, with the low-frequency ac electric field applied the induced electrostatic particle−surface interaction force has been estimated to be about 10.5 pN at a location of 20 nm from the gold nanopillar as depicted in Figure S4, which is 32 times larger than the peak repulsive thermophoretic force at the same location. The particle surface interaction force increases as the nanodiamond approaches the gold nanopillar surface, but it is eventually balanced by the electrical double-layer repulsion force to enable the nanodiamond to reach an equilibrium height from the gold nanopillar surface and prevent the nanodiamond from spontaneously sticking to the gold nanopillar surface. This equilibrium height is estimated to be approximately 20 nm from the surface of the gold nanopillar as depicted in Figure S4a. Thus, in LFET the electrostatic particle−surface interaction force induced by applying a low-frequency ac electric field conveniently overcomes the repulsive thermopho-retic force to still enable the trapping and dynamic manipulation of a single nanodiamond despite the repulsive thermophoretic force. Furthermore, the LFET approach allows us to achieve high stability trapping at low laser power (1 mW), which is smaller than the previously reported powers of 50−100 mW using a laser beam optical trap for the same size of single nanodiamond (~100 nm).[30,31]

The trapping stability remains approximately the same when the nanodiamond is trapped at the center of the pattern or near the edge of the nanopillar array as shown in Figure S6 of the Supporting Information. To verify single nanodiamond trapping, the trapped nanodiamond is patterned onto the gold nanopillar array and observed under scanning electron microscope (SEM). The diameter of the trapped nanodiamond is about 100 nm, as shown in the SEM image depicted in Figure S7 of the Supporting Information.

https://doi.org/10.1021/acs.nanolett.1c00357
Nano Lett. XXXX, XXX, XXX−XXX

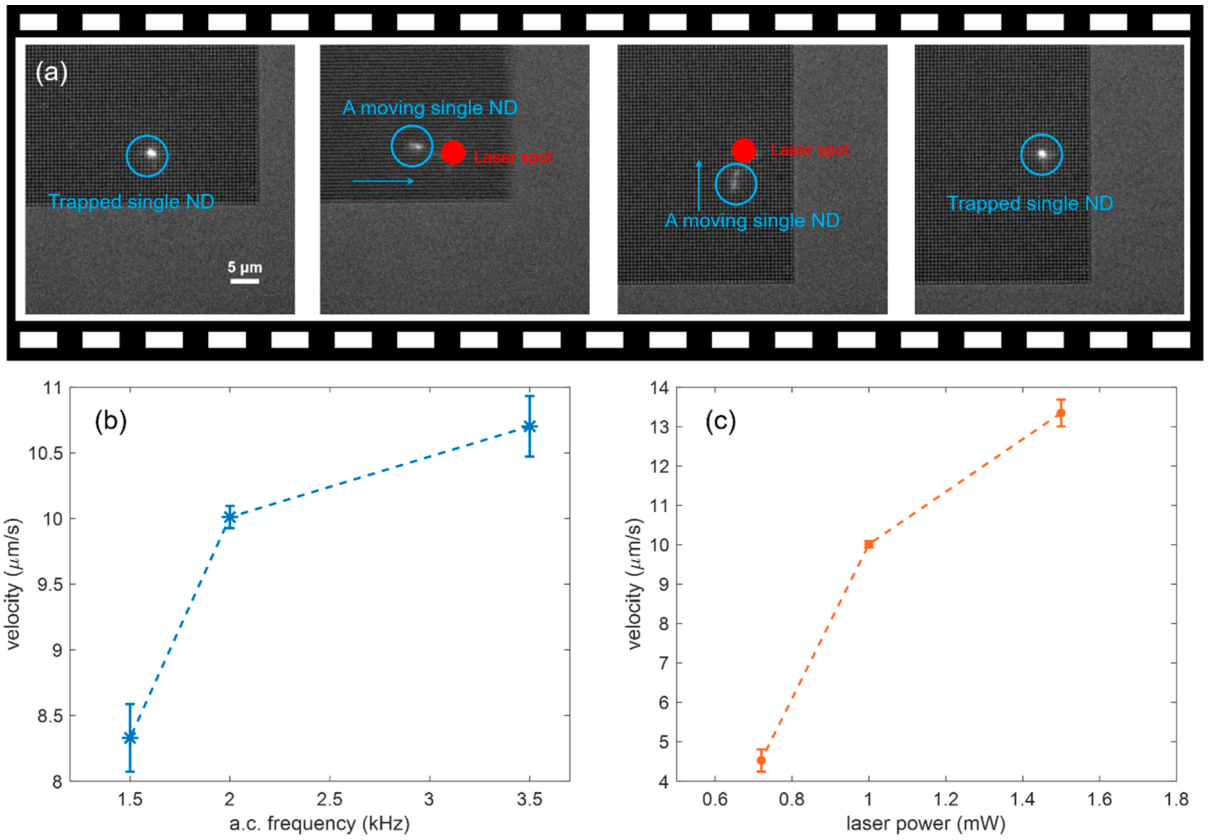

Figure 4. (a) The frame-by-frame sequence showing a single ND is stably trapped and manipulated along the gold nanopillar array using 1 mW laser power and a low-frequency ac field of 2 kHz. After both laser and ac field are turned on, a single ND is transported toward the illuminated spot within a few seconds. Subsequently, the laser spot is translated toward the right and the single ND moves rapidly toward the new laser spot and is stably trapped at the new location. (b,c) Transport velocity of the trapped nanodiamond under various ac frequency and laser power conditions. Blue asterisks represent the velocities under laser power from 0.72 to 1.5 mW with 2 kHz ac frequency. Orange dots represent the velocities under ac frequency for 1.5, 2, and 3.5 kHz with 1 mW laser power. For the same experimental condition, we repeated the experiment several times to calculate the average velocity. Error bars indicate the standard deviation of all the acquired velocities under the same experimental condition.

Besides trapping and releasing the NDs, the dynamic manipulation of the trapped NDs can be achieved using LFET, a capability not feasible in conventional chip-based plasmonic traps[3,5] based on near-field optical force alone or geometry-induced electrostatic traps.[32] The dynamic manipulation of the trapped NDs is achieved by translating the microscope stage or the laser beam focus along the in-plane direction. The translation of the laser focus from one position to another along the nanopillar array creates new thermal hotspots and hence new ETP flow that rapidly convects the trapped NDs to the newly illuminated spot along the surface of the nanopillar array as demonstrated in Figure 4a and SI Video 2. The manipulation can be achieved over the whole patterned region as long as the laser spot is kept on the nanopillar array. The velocity of the transport of the nanodiamond depends on the laser power and ac frequency. To clarify, as shown in the second and third frames of Figure 4 the single nanodiamond is not necessarily always within the laser spot during the motion of the laser spot illumination across the nanopillar array. When the laser spot is suddenly translated to another position, due to the contribution from ETP flow the single nanodiamond is delivered to the new laser spot site rapidly. We have also presented data on the average velocity of the nanodiamond transport given by the displacement between the initial laser spot and final laser spot position divided by the time span that the single nanodiamond takes to arrive at the new location of the laser spot. Higher laser power generates more photothermal-heating, so that the ETP flow is accelerated and the transport velocity is enhanced as depicted in Figure 4. For example, the transport velocity increases from 4.5 to 13.2 μm/s when the laser power was increased from 0.72 to 1.5 mW. With respect to variation of ac frequency, the nanodiamond transport velocity reduces with decreasing ac field frequency. We attribute this observation to the stronger electrostatic particle−surface force that increases with decreasing ac field frequency, resulting in more frictional drag on the nanodiamond as the ac frequency is reduced as depicted in Figure 4b,c. For all of the experimental conditions, the achieved transport velocity ranges from 4 to 14 μm/s. This ability to quickly deliver the nanodiamond to the position of the laser spot enables facile dynamic manipulation across the surface of the fold nanopillar array. In SI Video 4, we show a typical video used for calculating the transport velocity.

In conclusion, we have demonstrated a low-frequency electrothermoplasmonic tweezer that harnesses low-frequency ac electric field below 5 kHz combined with low laser power for the dynamic manipulation of single NDs along a gold nanopillar array substrate. The ability of our nanotweezer to trap a single ND within a few seconds and rapidly relocate it on a plasmonic substrate holds promise for the implementation of on-chip single photon sources, plasmonic nanolasers, and low-noise quantum sensors.

https://doi.org/10.1021/acs.nanolett.1c00357
Nano Lett. XXXX, XXX, XXX−XXX

METHODS

Gold Nanopillar Array Fabrication. After a float glass substrate was cleaned up, we deposited 50 nm of gold film with 5 nm of chromium as the adhesion layer. Then, photoresist (PMMA A4) was spin-coated on for electron beam lithography to define the pattern region. After development, another layer of 150 nm gold was deposited. Finally, we finished the process using acetone for lift-off, and a square gold nanopillar array with 80 μm on the side was left on the chip.

Sample Preparation. After the nanopillar was fabricated, we sandwiched the gold film by covering it with a glass coverslip that has a thin coating of indium tin oxide spaced by a 120 μm thick dielectric spacer to create a microfluidic channel around the patterns. Two copper wires are connected to the ITO side on the coverslip and on the gold film to apply the ac electric field.

The fluorescent nanodiamond solution originally had a concentration of 1 mg/mL in deionized water with nitrogen vacancy of ∼3 ppm and purchased at Sigma-Aldrich. The nanodiamond was diluted by 100 000 times using deionized water to generate a sparse enough solution suitable for single nanodiamond manipulation. The final concentration used in the experiment was 5.65×10^5 particle/mL.

Fluorescence Imaging. The trapping and imaging were performed using a custom fluorescent imaging and optical trapping microscope based on a Nikon Ti2-E inverted microscope. The suspended particle solution was injected into the microfluidic channel. A high quantum efficiency sCMOS camera (Photometrics PRIME 95B) was used to acquire images at a frame rate of 3.3333 frames per second. The trapped nanodiamonds were excited under a green light from a filtered broadband fluorescent illumination lamp (Nikon INTENSILIGHT C-HGFI). The emitted red light was collected through the same objective lens and imaged on the camera. The nanopillar array was illuminated with a 973 nm semiconductor diode laser (Thorlabs CLD1015). The laser beam was focused with a Nikon 60× water-immersion objective lens (NA, 1.2). The ac electric field was supplied by a dual-channel function generator (BK Precision 4047B).

ASSOCIATED CONTENT

Supporting Information

The Supporting Information is available free of charge at https://pubs.acs.org/doi/10.1021/acs.nanolett.1c00357.

Video showing the ability of a low-frequency electrothermoplasmonic trap to rapidly trap a single nanodiamond and to release the trapped single ND by increasing the ac frequency (AVI)

Video showing that after the single ND is trapped a dynamic manipulation is able to be achieved by translating the laser spot across the nanopillar array (AVI)

Video showing the recorded process of a trapped nanodiamond escaping from the trap when the ac field is turned off (AVI)

Video showing typical video frames used for measuring the average manipulation velocity of the nanodiamond (AVI)

Video showing a trapped nanodiamond near the edge of the pattern, corresponding to the data in Figure S6 (AVI)

The ac field with various sizes, force illustration and particle−surface interaction, ac osmosis simulation, stiffness analysis, SEM of deposited nanodiamond, thermal simulation from FEM software, balance between thermophoretic force and optical gradient force, full explanations of supporting videos (PDF)

AUTHOR INFORMATION

Corresponding Author

Justus C. Ndukaife − *Vanderbilt Institute of Nanoscale Science and Engineering, Vanderbilt University, Nashville, Tennessee 37212, United States; Department of Electrical Engineering and Computer Science, Vanderbilt University, Nashville, Tennessee 37212, United States;* orcid.org/0000-0002-8524-0657; Email: justus.ndukaife@vanderbilt.edu

Authors

Chuchuan Hong − *Vanderbilt Institute of Nanoscale Science and Engineering, Vanderbilt University, Nashville, Tennessee 37212, United States; Department of Electrical Engineering and Computer Science, Vanderbilt University, Nashville, Tennessee 37212, United States;* orcid.org/0000-0002-1329-9385

Sen Yang − *Vanderbilt Institute of Nanoscale Science and Engineering, Vanderbilt University, Nashville, Tennessee 37212, United States; Interdisciplinary Material Science, Vanderbilt University, Nashville, Tennessee 37212, United States;* orcid.org/0000-0002-0056-3052

Ivan I. Kravchenko − *Center for Nanophase Materials Sciences, Oak Ridge National Laboratory, Oak Ridge, Tennessee 37831, United States*

Complete contact information is available at: https://pubs.acs.org/10.1021/acs.nanolett.1c00357

Notes

The authors declare no competing financial interest.

ACKNOWLEDGMENTS

The authors acknowledge financial support from the National Science Foundation (NSF ECCS-1933109) and Vanderbilt University. A portion of this research was conducted at the Center for Nanophase Materials Sciences, which is a DOE Office of Science User Facility.

REFERENCES

(1) Ndukaife, J. C.; Xuan, Y.; Nnanna, A. G. A.; Kildishev, A. V.; Shalaev, V. M.; Wereley, S. T.; Boltasseva, A. High-Resolution Large-Ensemble Nanoparticle Trapping with Multifunctional Thermoplasmonic Nanohole Metasurface. *ACS Nano* **2018**, *12* (6), 5376−5384.

(2) Hong, C.; Yang, S.; Ndukaife, J. C. Optofluidic Control Using Plasmonic TiN Bowtie Nanoantenna. *Opt. Mater. Express* **2019**, *9* (3), 953−964.

(3) Wang, K.; Crozier, K. B. Plasmonic Trapping with a Gold Nanopillar. *ChemPhysChem* **2012**, *13* (11), 2639−2648.

(4) Gao, D.; Ding, W.; Nieto-Vesperinas, M.; Ding, X.; Rahman, M.; Zhang, T.; Lim, C.; Qiu, C.-W. Optical Manipulation from the Microscale to the Nanoscale: Fundamentals, Advances and Prospects. *Light: Sci. Appl.* **2017**, *6* (9), e17039−e17039a.

(5) Wang, K.; Schonbrun, E.; Steinvurzel, P.; Crozier, K. B. Trapping and Rotating Nanoparticles Using a Plasmonic Nano-Tweezer with an Integrated Heat Sink. *Nat. Commun.* **2011**, *2* (1), 469.

(6) Juan, M. L.; Righini, M.; Quidant, R. Plasmon Nano-Optical Tweezers. *Nat. Photonics* **2011**, *5* (6), 349−356.

(7) Crozier, K. B. Quo Vadis, Plasmonic Optical Tweezers? *Light: Sci. Appl.* **2019**, *8* (1), 35.
(8) Pang, Y.; Gordon, R. Optical Trapping of 12 Nm Dielectric Spheres Using Double-Nanoholes in a Gold Film. *Nano Lett.* **2011**, *11* (9), 3763−3767.
(9) Juan, M. L.; Gordon, R.; Pang, Y.; Eftekhari, F.; Quidant, R. Self-Induced Back-Action Optical Trapping of Dielectric Nanoparticles. *Nat. Phys.* **2009**, *5* (12), 915−919.
(10) Mestres, P.; Berthelot, J.; Aćimović, S. S.; Quidant, R. Unraveling the Optomechanical Nature of Plasmonic Trapping. *Light: Sci. Appl.* **2016**, *5* (7), e16092−e16092a.
(11) Rodiek, B.; Lopez, M.; Hofer, H.; Porrovecchio, G.; Smid, M.; Chu, X.-L.; Gotzinger, S.; Sandoghdar, V.; Lindner, S.; Becher, C.; Kuck, S. Experimental Realization of an Absolute Single-Photon Source Based on a Single Nitrogen Vacancy Center in a Nanodiamond. *Optica* **2017**, *4* (1), 71.
(12) Chi, Y.; Chen, G.; Jelezko, F.; Wu, E.; Zeng, H. Enhanced Photoluminescence of Single-Photon Emitters in Nanodiamonds on a Gold Film. *IEEE Photonics Technol. Lett.* **2011**, *23* (6), 374−376.
(13) Cuche, A.; Drezet, A.; Sonnefraud, Y.; Faklaris, O.; Treussart, F.; Roch, J.-F.; Huant, S. Near-Field Optical Microscopy with a Nanodiamond-Based Single-Photon Tip. *Opt. Express* **2009**, *17* (22), 19969.
(14) Bogdanov, S. I.; Boltasseva, A.; Shalaev, V. M. Overcoming Quantum Decoherence with Plasmonics. *Science (Washington, DC, U. S.)* **2019**, *364* (6440), 532−533.
(15) Lin, L.; Wang, M.; Peng, X.; Lissek, E. N.; Mao, Z.; Scarabelli, L.; Adkins, E.; Coskun, S.; Unalan, H. E.; Korgel, B. A.; Liz-Marzán, L. M.; Florin, E.-L.; Zheng, Y. Opto-Thermoelectric Nanotweezers. *Nat. Photonics* **2018**, *12* (4), 195−201.
(16) Vigolo, D.; Buzzaccaro, S.; Piazza, R. Thermophoresis and Thermoelectricity in Surfactant Solutions. *Langmuir* **2010**, *26* (11), 7792−7801.
(17) Iacopini, S.; Piazza, R. Thermophoresis in Protein Solutions. *Europhys. Lett.* **2003**, *63* (2), 247−253.
(18) Piazza, R.; Parola, A. Thermophoresis in Colloidal Suspensions. *J. Phys.: Condens. Matter* **2008**, *20* (15), 153102.
(19) Ghosh, S.; Ghosh, A. All Optical Dynamic Nanomanipulation with Active Colloidal Tweezers. *Nat. Commun.* **2019**, *10* (1), 4191.
(20) Hong, C.; Yang, S.; Ndukaife, J. C. Stand-off Trapping and Manipulation of Sub-10 Nm Objects and Biomolecules Using Opto-Thermo-Electrohydrodynamic Tweezers. *Nat. Nanotechnol.* **2020**, *15* (11), 908−913.
(21) Ndukaife, J. C.; Kildishev, A. V.; Nnanna, A. G. A.; Shalaev, V. M.; Wereley, S. T.; Boltasseva, A. Long-Range and Rapid Transport of Individual Nano-Objects by a Hybrid Electrothermoplasmonic Nanotweezer. *Nat. Nanotechnol.* **2016**, *11* (1), 53−59.
(22) Ndukaife, J. C.; Shalaev, V. M.; Boltasseva, A. Plasmonics–Turning Loss into Gain. *Science (Washington, DC, U. S.)* **2016**, *351* (6271), 334−335.
(23) Hatlo, M. M.; Lue, L. The Role of Image Charges in the Interactions between Colloidal Particles. *Soft Matter* **2008**, *4* (8), 1582.
(24) Sarshar, M.; Wong, W. T.; Anvari, B. Comparative Study of Methods to Calibrate the Stiffness of a Single-Beam Gradient-Force Optical Tweezers over Various Laser Trapping Powers. *J. Biomed. Opt.* **2014**, *19* (11), 115001.
(25) Morgan, H.; Green, N. G. AC Electrokinetics. In *Encyclopedia of Microfluidics and Nanofluidics*; Springer US: Boston, MA, 2002; pp 8−8a.
(26) Ramos, A.; Morgan, H.; Green, N. G.; Castellanos, A. Ac Electrokinetics: A Review of Forces in Microelectrode Structures. *J. Phys. D: Appl. Phys.* **1998**, *31* (18), 2338−2353.
(27) Duhr, S.; Braun, D. Why Molecules Move along a Temperature Gradient. *Proc. Natl. Acad. Sci. U. S. A.* **2006**, *103* (52), 19678−19682.
(28) Shoji, T.; Shibata, M.; Kitamura, N.; Nagasawa, F.; Takase, M.; Murakoshi, K.; Nobuhiro, A.; Mizumoto, Y.; Ishihara, H.; Tsuboi, Y. Reversible Photoinduced Formation and Manipulation of a Two-Dimensional Closely Packed Assembly of Polystyrene Nanospheres on a Metallic Nanostructure. *J. Phys. Chem. C* **2013**, *117* (6), 2500−2506.
(29) Roxworthy, B. J.; Ko, K. D.; Kumar, A.; Fung, K. H.; Chow, E. K. C.; Liu, G. L.; Fang, N. X.; Toussaint, K. C. Application of Plasmonic Bowtie Nanoantenna Arrays for Optical Trapping, Stacking, and Sorting. *Nano Lett.* **2012**, *12* (2), 796−801.
(30) Horowitz, V. R.; Aleman, B. J.; Christle, D. J.; Cleland, A. N.; Awschalom, D. D. Electron Spin Resonance of Nitrogen-Vacancy Centers in Optically Trapped Nanodiamonds. *Proc. Natl. Acad. Sci. U. S. A.* **2012**, *109* (34), 13493−13497.
(31) Neukirch, L. P.; Gieseler, J.; Quidant, R.; Novotny, L.; Nick Vamivakas, A. Observation of Nitrogen Vacancy Photoluminescence from an Optically Levitated Nanodiamond. *Opt. Lett.* **2013**, *38* (16), 2976.
(32) Krishnan, M.; Mojarad, N.; Kukura, P.; Sandoghdar, V. Geometry-Induced Electrostatic Trapping of Nanometric Objects in a Fluid. *Nature* **2010**, *467* (7316), 692−695.

https://doi.org/10.1021/acs.nanolett.1c00357
Nano Lett. XXXX, XXX, XXX−XXX